ELSEVIER

Int. J. Therm. Sci. 41 (2002) 517–527

International Journal of Thermal Sciences

www.elsevier.com/locate/ijts

A numerical study for the estimation of a convection heat transfer coefficient during a metallurgical "Jominy end-quench" test ☆

Philippe Le Masson [a,*], Tahar Loulou [b], Eugène Artioukhine [c], Philippe Rogeon [a], Denis Carron [a], Jean-Jacques Quemener [a]

[a] *LETEE (Laboratoire d'Études Thermiques Énergétiques et Environnement), Université de Bretagne-Sud, Centre de Recherches, Rue St. Maude, 56325 Lorient cedex, France*

[b] *Centre Energétique Environnement, Ecole des Mines d'Albi, Carmaux, F-81013 Albi, France*

[c] *CREST – IGE, Université de Franche Comté, Parc Technologique, 2 Avenue Jean Moulin, F-90000 Belfort, France*

Received 2 October 2001; accepted 18 March 2002

Abstract

A numerical method for the two-dimensional estimation of a convection heat transfer coefficient is developped for a rapid metallurgical heat treatment: the "Jominy end-quench" test. The estimation algorithm is based on the iterative regularization method and on the conjugate gradient and adjoint methods. The procedure is verified for two different materials. The first material, the Nickel, has no metallurgic transformation. The second one, the 16MND5 steel, has transformations implying high nonlinearities in the material. The estimation is simulated numerically for three types of heat transfer coefficients and theoritical thermal cycles. One of these coefficients can be brought together with an experimental case. For the noised thermal cycles the solution is stabilized by the iterative regularization.

Keywords: Inverse method; Iterative regularization; Conjugate gradient; Jominy end-quench test; Thermo-metallurgical modelisation; 16MND5 stell; Nickel

1. Introduction

The numerical simulation of rapid metallurgical transformations occured during some specific heat treatments (weld, quench: "Jominy end-quench") requires a good knowledge of the heat transfer conditions at the boundaries of the considered domain. The direct measurement of these conditions is impossible and it is necessary to solve an inverse heat transfer problem to estimate them. In a previous work, we have used the finite element code SYSWELD [1] to examine the parametrically of the Jominy end quench test. Meshing, metallurgic transformation enthalpy, Continuous Cooling Transformation (CCT) diagram modelling, emissivity of the surfaces and lower side transfer coefficient have been considered. The study was used to analyze the sensitivity of the numerical results regarding thermal kinetics, hardness and phase proportions [2]. This numerical simulation had been validated with experimental tests. At the same time, the heat transfer coefficient on the lower side of the sample was specifically studied by solving a 2-D inverse problem [3]. In the literature, we have just find three publications upon inverse estimations of "Jominy end-quench" test. The first [4] is an inverse estimation of transient heat transfer coefficients in a 1D quenching problem with the sequential function specification method. The second [5] is an estimation of the heat flux and the temperature distribution in a 2D linear problem with the iterative regularization method. The third [6] use the specification function method in 1D quenching problem with a coupled thermo-metallurgical problem. We can see on the errors of estimates that we have oscillations during the phase transformations.

The estimation in the paper [3] was based on the function specification method using future temperatures [7] and on the spatial regularization method [8–10]. The results show the influence of metallurgic transformations (change from an austenitic phase to a martensitic phase). Like as [6], the dissipated heat and the evolution of conductivities

☆ This article is a follow up a communication presented by the authors at the EUROTHERM Seminar 68, "Inverse problems and experimental design in thermal and mechanical engineering", held in Poitiers in March 2001.

* Correspondence and reprints.

E-mail addresses: philippe.le-masson@univ-ubs.fr (P. Le Masson), loulou@enstimac.fr (T. Loulou), artioukhine@ige.univ-fcomte.fr (E. Artioukhine).

1290-0729/02/$ – see front matter
PII: S1290-0729(02)01345-5

Nomenclature

a	diffusivity	$m^2 \cdot s^{-1}$	
Ci	specific heat of the phase i		
D^n	vector of descent direction		
dT/dt	variation of the temperature with time	$K \cdot s^{-1}$	
ΔFo	$= \frac{a\Delta t}{z^2}$ delta fourier		
H_γ, H_α	enthalpies of the phases γ and α	$J \cdot m^{-3}$	
$H(r,t)$, H^{n+1}	heat transfer coefficient	$W \cdot m^{-2} \cdot K^{-1}$	
HRC	rockwell C hardness		
$J(H)$	residual functional		
∇J^n	the gradient of the residual functional		
L_{ij}, $L_{\gamma\alpha}$	heat transformation of phase i to j	$J \cdot m^{-3}$	
n, n^*	iteration number, last iteration		
P_i, P, P_{eq}	proportion of metallurgic phase		
r	spatial coordinates	m	
T_{inf}	external temperature	°C	
T_{water}	temperature of water	°C	
T, T_i	temperature in the sample	°C	
T_0, T_{max}	initial and maximal temperatures in the sample	°C	
Y, Y_i, Y_e	experimental temperatures	°C	
z	spatial coordinates	m	
γ^n	descent parameter		
δ^2	convergence criterion		
$\varepsilon(T)$	emissivity of the sample		
ε_1	arrest criterion		
λ_i	conductivity of the phase i	$W \cdot m^{-1} \cdot K^{-1}$	
ρ_i	density of the phase i	$Kg \cdot m^{-3}$	
σ^2	root-mean-square error on the temperature		
ω	a random number		
Δ_{max}	the magnitude of the disturbance		
$\theta(z,r,t)$	temperature variation		
$\Psi(z,r,t)$	adjoint variable		

(Fig. 1) during the transformation generate oscillations in the estimate. In order to overcome this difficulty, we apply in this paper the iterative regularization method [11–13]. A similar method has been applied by Abou Kachefe and Jarny [14].

Here, we use the Iterative Regularization Method "IRM" for the 2D nonlinear axysymetrique problem in the Jominy end-quench test. In fine, the difficulty of the studies is the simulation of the coupled thermometallurgical problem with high nonlinearities (principally on the conductivity during the phase transformation—austenite martensite).

First we present the Jominy end-quench test, as developed at the LET2E laboratory, and the sample modelling. Second, the estimation method is discussed. This method being formulated in cylindrical coordinates, it leads us to express and analyze two types of adjoint systems. Finally, two materials (with and without transformations) are used to verify the method for some test cases. The used theoretical thermal cycles are considered at dimensions smaller than $z = 1$ mm in relation to the surface studied, and a noise is added. The inverse problem with temperatures at $z = 0$ mm is considered like as a pseudo-inverse problem. However, with this test case it is possible to validate the estimation code.

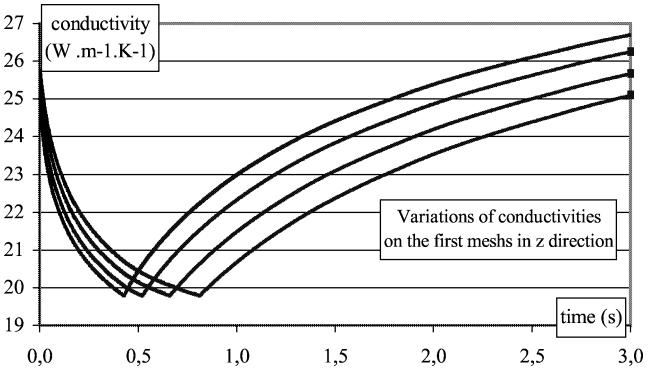

Fig. 1. Conductivity variations.

2. Jominy end-quench test

2.1. Principle

The Jominy end quench test is a standard test (NF A 04-303) used to characterize hardenability of steel [15,16]. A steel cylinder (diameter: 25 mm; length: 100 mm) is heated within the austenitic domain during a preset time and cooled by a water jet on its lower end (for NF A 04-303, T_{water} must be between 15 and 25 °C) (Fig. 2). After cooling the Jominy bar is polished parallel to the cylinder axis on both sides. Hardness measurements are carried out along the cylinder axis as a function of distance from the quenched extremity (1.5 mm, 3 mm, 5 mm, 7 mm, 9 mm, 11 mm,

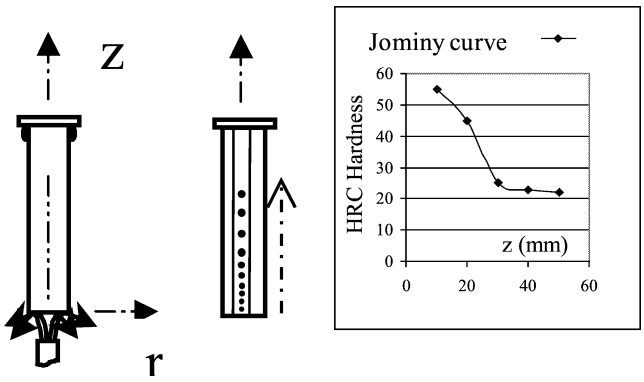

Fig. 2. Jominy test: Cooling, Hardness measurement and Jominy hardenability curve.

..., 60 mm, 70 mm and 80 mm). The curve representing the hardness variations vs. the distance from the quenched end of the cylinder is called the Jominy hardenability curve.

2.2. The Jominy test at the laboratory

The experimental set-up in accordance with the standard present several characteristics:

- Induction heating in an inert gas (argon) filled enclosure;
- Computer-aided management of the various actions (heating, cylinder handling, quenching), thanks to which the reproducibility is satisfactory;
- Thermal kinetics follow up through the embedding of thermocouples in relevant places (under the lower side and on the lateral surface), which makes it possible using inverse methods to identify parameters.

2.3. Numerical simulation of the Jominy test

The numerical simulation is conducted from a fully austenitized 16MND5 steel sample heated at 880 °C. The equations, implemented in both the SYSWELD code and the estimation code we developed, are the heat conduction equation (1) and the metallurgical kinetic equations (2) of the type Leblond and Devaux [17] and Koistinen and Marburger [18]. The study domain (radial plane) is defined in cylindrical coordinates assuming the problem to be axisymmetric:

$$\sum_i P_i \rho_i(T) C_i(T) \frac{\partial T}{\partial t} = \frac{1}{r}\frac{\partial}{\partial r}\left(r \sum_i P_i \lambda_i(T) \frac{\partial T}{\partial r}\right) + \frac{\partial}{\partial z}\left(\sum_i P_i \lambda_i(T) \frac{\partial T}{\partial z}\right) - \sum_{i<j} P_{ij} L_{ij} \tag{1}$$

$$\frac{\mathrm{d}P}{\mathrm{d}t} = \frac{P_{\mathrm{eq}} - P}{\tau} f\left(\frac{\mathrm{d}T}{\mathrm{d}t}\right) \quad \text{and}$$

$$P = P_{\max}\left(1 - \exp\left(-b(Ms - T)\right)\right) \tag{2}$$

In the heat conduction equation, a source term allows to considerate the phase change enthalpy $L\gamma\alpha$ according to the temperature during the sample cooling. The heat of transformation is calculated according to the phase enthalpy: $L\gamma\alpha = H_\gamma - H_\alpha$ and by considering two metallurgical phases only: γ (austenite) and α (ferrite, pearlite, bainite or martensite). The enthalpies of the phase α and γ are defined by polynomial functions between 100 °C and 1450 °C. We define the parameters of the metallurgical kinetics equations with the simulation of the CCT diagram (Fig. 3). For each time and point, we take the speed cooling and the temperature of the point. With these two informations, we can have the percentage P_i of the metallurgical transformation.

Moreover, the thermophysical characteristics $\rho(T)$, $C(T)$ and $\lambda(T)$ are calculated at all time steps by a law of mixtures

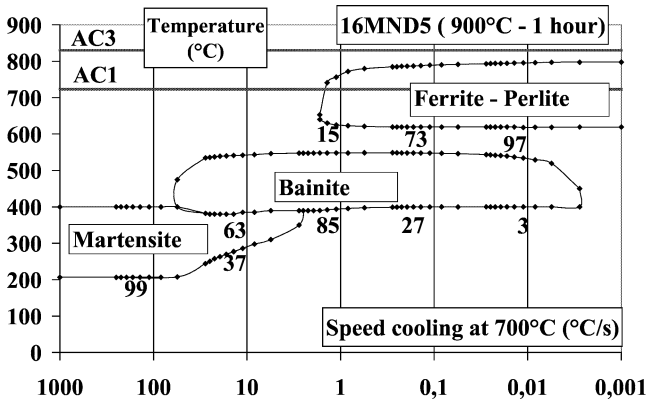

Fig. 3. Simulation of the CCT diagram.

according to the temperature (ex: $\lambda(T) = P_\gamma \cdot \lambda_\gamma(T) + P_\alpha \cdot \lambda_\alpha(T) = \sum_i P_i \lambda_i(T)$).

The boundary and initial conditions are the following:

Lower side:

$$-\sum_i P_i \lambda_i(T) \frac{\partial T(z=0,r,t)}{\partial z} = H(r,T)\left[T(0,r,t) - T_{\mathrm{water}}\right] \tag{3}$$

Upper side:

$$\frac{\partial T(z_{\max},r,t)}{\partial z} = 0 \tag{4}$$

Lateral surface:

$$-\sum_i P_i \lambda_i(T) \frac{\partial T(z,r_{\max},t)}{\partial r} = \varepsilon(T)\sigma\left[T^4(z,r_{\max},t) - T_{\mathrm{inf}}^4\right] \tag{5}$$

Convection is estimated negligible compared to radiation on the lateral surface. We have estimated a radiatif coefficient at around 80 $\mathrm{W{\cdot}m^{-2}{\cdot}K^{-1}}$ and a convection coefficient lower 10 $\mathrm{W{\cdot}m^{-2}{\cdot}K^{-1}}$. In fact, we define a global heat transfer coefficient on the lateral surface.

On the axis:

$$\frac{\partial T(z,r=0,t)}{\partial r} = 0 \tag{6}$$

Initial values:

$$T(z,r,0) = T_0; \quad P\gamma(r,z,0) = 1 \tag{7}$$

The data set making up the model is:

- The mesh;
- The thermophysical characteristics $\rho(T)$, $C(T)$, $\lambda(T)$ and $L_{\alpha\gamma}$ for the different phases according to the temperature;
- The transformation initial and final temperatures of all phases (CCT diagram);
- The initial temperature $T_0 = 880\,^\circ\mathrm{C}$ throughout the whole sample;
- The external temperature T_{inf} and the temperature of water: T_{water};

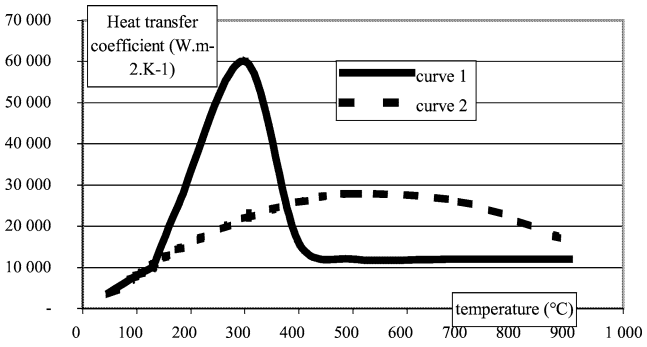

Fig. 4. Hypotheses for the heat transfer coefficients.

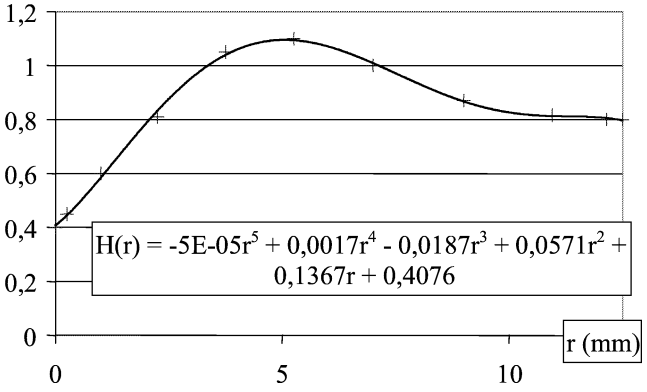

Fig. 5. Weighting curve of the transfer coefficient vs. radius.

- The emissivity of the material considered constant and equal to 0.8;
- Finally, during the perfecting of the computing programs, two hypotheses are assumed for the heat transfer coefficient (Fig. 4). The first hypothesis, by Sorin [19] (*curve* 1), involves the presence of vaporization, boiling and forced convection on the surface according to the level of the temperature. In the second hypothesis, by Homberg [20] (*curve* 2), a coefficient less dependent from the temperature is assumed. The 2 hypotheses are based on the global analysis of the lower surface. For the purpose of this study, we choose Sorin's hypothesis where the variations of coefficients are higher. And we have attempted here to take into account a heat transfer coefficient varying not only with temperature of lower surface but also with the radius. When examining the water jet on the lower side, we can consider a point or a surface arrest in the centre (in $r = 0$) and, then, a heat transfer coefficient depending on the radius (Fig. 5). Fig. 6 shows the result of this heat transfer coefficient.

These equations are solved by the fine discretization of the domain near $z = 0$ ($\Delta r = 0.05$ mm; $\Delta z = 0.1$ mm) by taking into account the heat flow loss from the lower side, on the one hand, and by using a finite volume method, on the other hand.

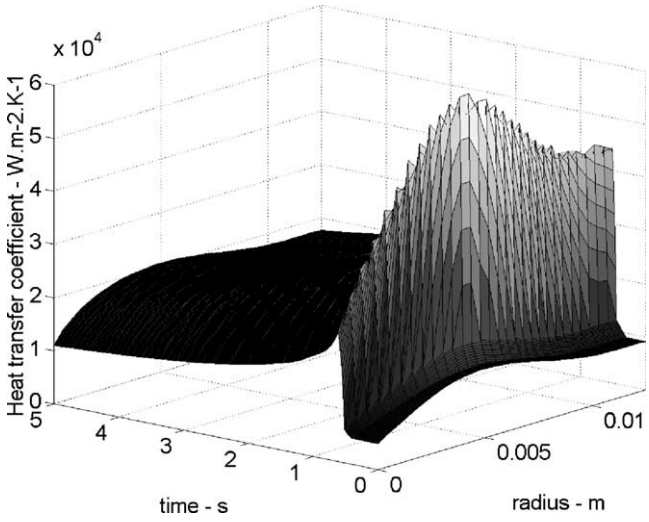

Fig. 6. Theoretical values of the transfer coefficient.

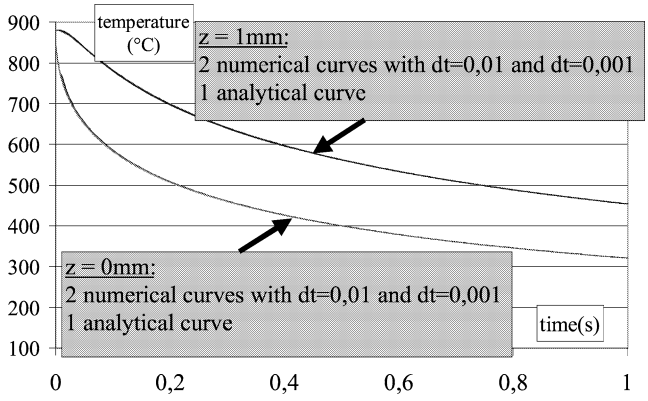

Fig. 7. Comparison of analytical and numerical solutions.

The numerical model was verified using an analytical method of the integral transform type [21] with constant thermophysical characteristics. This preliminary study makes it possible to verify the mesh with regard to the heat transfer coefficient values, the computation time step and the solution algorithm of the direct problem (this algorithm is afterward also used for variation and adjoint problems). Fig. 7 presents the thermal kinetics achieved with a constant heat transfer coefficient equal to 15 000 $\mathrm{W{\cdot}m^{-2}{\cdot}K^{-1}}$.

3. Estimation of the transfer coefficient—minimization procedure

The objective of this research is to determine the heat transfer coefficient on the lower side of the sample according to both time and radius: $H(r,t)$. The determination is conducted from the temperature values taken at a depth smaller or equal to $z = 1$ mm.

The estimation of the transfer coefficient in view of the direct problem (Eqs. (1)–(7)) can be formulated under

the variational form which implies the residual functional minimization

$$J(H)=\int_0^{t_f}\sum_{i=1}^{N}\left[T(z_i,r_i,t;H)-Y(z_i,r_i,t)\right]^2\mathrm{d}t \tag{8}$$

where $T(z_i,r_i,t;H)$ and $Y(z_i,r_i,t)$ represent the estimate temperature and the temperature measured at N various points of the material, respectively. The inverse problem consists in minimizing this residual functional under constraints given by the equations of the direct system (Eqs. (1)–(7)).

The minimization is carried out by using the conjugate gradient method [22]. The function $H(r,t)$ is considered here as an element of the Hilbert space, L^2. In this iterative method, the new functions are obtained after each iteration as followes:

$$\boldsymbol{H}^{n+1}=\boldsymbol{H}^n+\gamma^n\boldsymbol{D}^n,\quad n=1,\ldots,n^* \tag{9}$$

Where n is the iteration index, n^* the index of the last iteration, γ^n the descent parameter, $\boldsymbol{H}^{n+1}$ the unknown vector to be estimated and $\boldsymbol{D}^n$ the vector of descent direction given by:

$$D^n=-\nabla J^n+\beta^n D^{n-1} \tag{10}$$

where

$$\beta^n=\frac{\langle\nabla J^n-\nabla J^{n-1},\nabla J^n\rangle}{\langle\nabla J^n,\nabla J^n\rangle},\qquad \beta^0=0 \tag{11}$$

with $\langle,\rangle$ is the scalar product in Hilbert space L^2.

In the absence of noise, the iteration procedure is carried on until the following stopping criterion is verified:

$$\left|\frac{(H^{n+1}-H^n)}{H^n}\right|\leqslant\varepsilon_1 \tag{12}$$

The gradient ∇J^n of the residual functional of Eqs. (10) and (11) is obtained for all values of r and t by the following analytical relationship [11]:

$$\nabla J^n=\Psi(0,r,t)^*\left(T(0,r,t)-T_{\mathrm{inf}}\right) \tag{13}$$

Where $\Psi(z=0,r,t)$ is the solution of the adjoint problem achieved during the integration of the Lagrange functional and of the following variation problem $(\theta(z,r,t))$:

$$\frac{\partial\left(\sum_i P_i\rho_i(T)C_i(T)\theta\right)}{\partial t}=\frac{1}{r}\frac{\partial}{\partial r}\left(r\frac{\partial\left(\sum_i P_i\lambda_i(T)\theta\right)}{\partial r}\right)+\frac{\partial}{\partial z}\left(\frac{\partial\left(\sum_i P_i\lambda_i(T)\theta\right)}{\partial z}\right)+\Delta P_{\gamma\alpha}\frac{\partial}{\partial T}(\rho_\alpha H_\alpha-\rho_\gamma H\gamma)\theta \tag{14}$$

$$\theta=0\quad t=0,\ 0<r<r_{\max},\quad 0<z<z_{\max} \tag{15}$$

$$\frac{\partial\theta}{\partial r}=0\quad r=0,\ 0<t<t_f,\ 0<z<z_{\max} \tag{16}$$

$$\frac{\partial\theta}{\partial z}=0\quad z=z_{\max},\ 0<t<t_f,\ 0<r<r_{\max} \tag{17}$$

$$-\frac{\partial\left(\sum_i P_i\lambda_i(T)\theta\right)}{\partial r}=\left(4\varepsilon\sigma T^3\right)\theta$$
$$r=r_{\max},\ 0<t<t_f,\ 0<z<z_{\max} \tag{18}$$

$$-\frac{\partial\left(\sum_i P_i\lambda_i(T)\theta\right)}{\partial z}=H(r,t)\theta+\delta H(r,t)(T-T_{\mathrm{water}})$$
$$z=0,\ 0<t<t_f,\ 0<r<r_{\max} \tag{19}$$

In this variation problem, $\delta H(r,t)$ is defined by $\delta H(r,t)=D^n(0,r,t)$ being the descent direction.

Two possibilities are at our disposal to obtain the adjoint problem: either multiplying Eq. (14) of the variation problem by r before integrating, or not. In the literature, Alifanov and Nenarokomov [13] give a solution where this product by r appears. In Alifanov and Kerov [12], on the other hand, the adjoint system in the case of a cylindrical linear problem is expressed without multiplying by r.

In the first case, we obtain:

$$-\sum_i P_i\rho_i(T)C_i(T)\frac{\partial\Psi}{\partial t}=\frac{1}{r}\frac{\partial}{\partial r}\left(r\sum_i P_i\lambda_i(T)\frac{\partial\Psi}{\partial r}\right)+\frac{\partial}{\partial z}\left(\sum_i P_i\lambda_i(T)\frac{\partial\Psi}{\partial z}\right)+\Psi\Delta P_{\gamma\alpha}\frac{\partial}{\partial T}(\rho_\alpha H_\alpha-\rho_\gamma H\gamma)+\sum_{j=1}^{N}\left[T(z_j,r_j,t)-Y(z_j,r_j,t)\right]\cdot\delta(r-r_i)\cdot\delta(z-z_i) \tag{20}$$

$$\Psi=0\quad t=t_f,\ 0<r<r_{\max},\ 0<z<z_{\max} \tag{21}$$

$$\frac{\partial\Psi}{\partial r}=0\quad r=0,\ 0<t<t_f,\ 0<z<z_{\max} \tag{22}$$

$$\frac{\partial\Psi}{\partial z}=0\quad z=z_{\max},\ 0<t<t_f,\ 0<r<r_{\max} \tag{23}$$

$$-\sum_i P_i\lambda_i(T)\frac{\partial\Psi}{\partial r}=\left(4\varepsilon\sigma T^3\right)\Psi$$
$$r=r_{\max},\ 0<t<t_f,\ 0<z<z_{\max} \tag{24}$$

$$-\sum_i P_i\lambda_i(T)\frac{\partial\Psi}{\partial z}=H\Psi$$
$$z=0,\ 0<t<t_f,\ 0<r<r_{\max} \tag{25}$$

In the second case, the system differs, in the main equation and in the boundary conditions, in the appearance of a term in Ψ/r, which, when writing the code for $r=0$, is problematic.

Thanks to the testing of both systems, we have been able to verify, as specified in reference [11], that the adjoint system can be written by different ways and that the adjoint variables calculated are accurate. The first system described above including the product by r is then used for the rest of the study.

Finally, the value of descent parameter γ^n is determined by the linear relationship [11]:

$$\gamma^n = -\sum_{i=1}^{N}\int_0^{t_f}\left[T(r_i,z_i,t)-Y(r_i,z_i,t)\right]\theta(r_i,z_i,t)\,\mathrm{d}t \times\left[\sum_{i=1}^{N}\int_0^{t_f}\left(\theta(r_i,z_i,t)\right)^2\mathrm{d}t\right]^{-1} \quad (26)$$

where $\theta(r,z,t)$ is the solution of the variation problem and N, the number of measurement points.

The three systems are solved numerically using a control volume method and an implicit scheme. The estimation procedure consists in:

(1) Defining the initial values of de $H^0(r,t)$;
(2) Solving the direct system: Eqs. (1)–(7);
(3) Calcultating the quadratic criterion $J(H)$: Eq. (8);
(4) Verifying the convergence criterion: Eq. (12);
(5) Solving the adjoint system: Eqs. (20)–(25);
(6) Calculating the gradient residual function: Eq. (13);
(7) Calculating the descent direction: Eqs. (10) and (11);
(8) Solving the variation problem: Eqs. (14)–(19);
(9) Calculating the descent parameter γ^n: Eq. (26);
(10) Incrementing the vector $H^{n+1}(r,t)$: Eq. (9);
(11) And back to step (2).

4. Regularization

The inverse problems are ill-posed and numerical solutions depend on the fluctuations occurring at the measurements. Small fluctuations at the measurements can generate big errors in the solution to be estimated. For the iterative regularization method [11], we introduce a convergence criterion δ^2 defined as:

$$\delta^2 = \int_0^{t_f}\sum_{i=1}^{N}\sigma^2(z_i,r_i,t)\,\mathrm{d}t \quad (27)$$

and so that $J(H) < \delta^2$ it possible to stop the iterative process with an acceptable solution. In the expression of δ^2, $\sigma^2(z,r,t)$ is the root-mean-square error on the temperature measurements achieved using smoothing techniques for the thermal cycles.

5. Application of the method

In order to validate the method, two materials have been used. One is nickel, without metallurgical transformations; the other is 16MND5 steel, the thermophysical characteristics $\rho(T)$, $\lambda(T)$ and $C(T)$ of which according to the phases and the temperature, as well as the CCT diagram considered as the basis of the transformations, are supposed to be known. The theoritical temperatures are taken at the dimensions $z = 0$ mm, $z = 0.6$ mm and $z = 1$ mm.

5.1. Case of nickel

As regards nickel only the heat transfer equation has to be solved. Two types of law have been tested in order to validate the code. The first law is $H(r,t) = 15\,000$ W·m^{-2}·K^{-1} (Fig. 8) and the second is a coefficient, which varies along a dome ($H(r,t) = 1\,000 + 7\,500\cdot(\sin(\pi t/t_{\max}) + \sin(\pi r/r_{\max}))$ (Fig. 10). The temperatures are taken at the depths $z = 0$ and $z = 1$ mm. In the absence of noise, the transfer coefficients are correctly found except near t_f where the initial condition of the adjoint problem sets the adjoint variable equal to zero and, therefore, implies that the gradient be always equal to zero. The more we are moving away from the surface ($z = 0$), the more the initial condition affects the estimate and increases the error.

Figs. 8–11 show the results achieved for both case with, for $z = 1$ mm, $\Delta Fo = a\Delta t/z^2 = 0.08$ and $N = 30$.

The analysis of the different estimates confirms that the errors are all the more big since we are moving away from the surface ($z = 0$) and especially when approaching $t = t_f$. Increasing the estimation domain by 15 to 30% beyond the effective time is taken.

Figs. 12(a) and (b) show the results in the case of the dome for a $-t_f' = t_f + 30\%$, b—truncated at t_f. The results are better.

In a second phase, we verify that, even in the presence of noise, the convergence of the code toward an estimation is acceptable. The case of the dome only, for which a noise has been added to the theoretical thermal cycles, is presented here. The disturbance is defined by the relationship: $B = \omega T_{\max}\Delta_{\max}$ where ω is a random number generator in $[-1,+1]$, $T_{\max}$ is the maximum value of the surface temperature and $\Delta_{\max}$ is the magnitude of the disturbance. For these numerical tests, we consider $T_{\max} = 880\,^{\circ}$C and $\Delta_{\max} = 5\%$.

$$Y_i(r_i,z_i,t) = Y_e(r_i,z_i,t) + \omega T_{\max}\Delta_{\max} \quad i = 1,\ldots,N \quad (28)$$

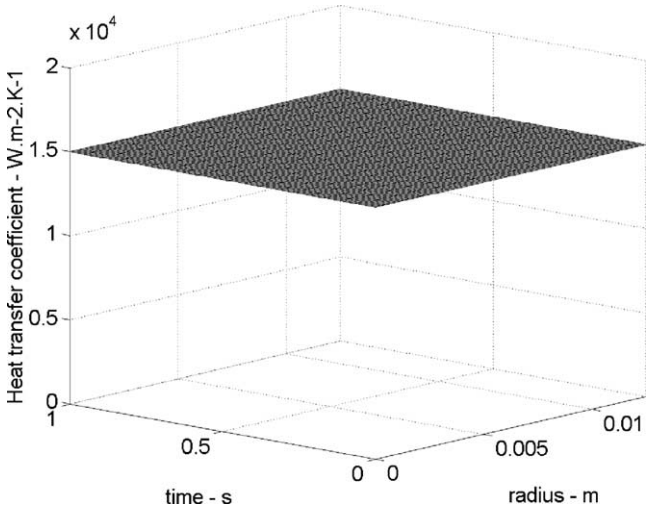

Fig. 8. Correct value to be estimated, case $H = 15\,000$ W·m^{-2}·K^{-1}.

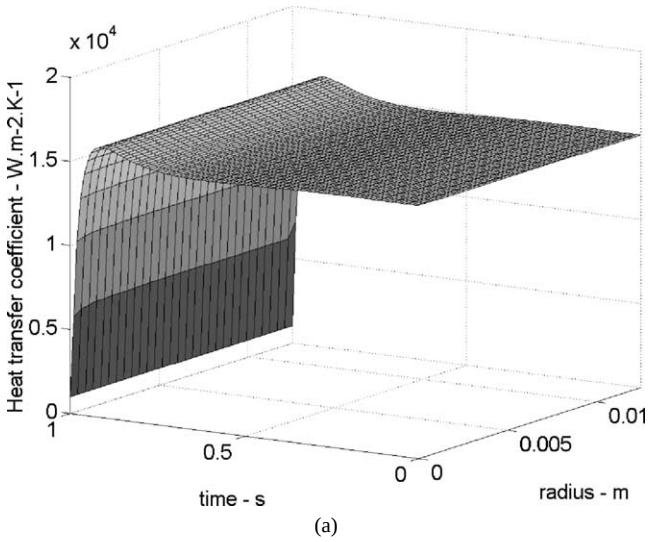

(a)

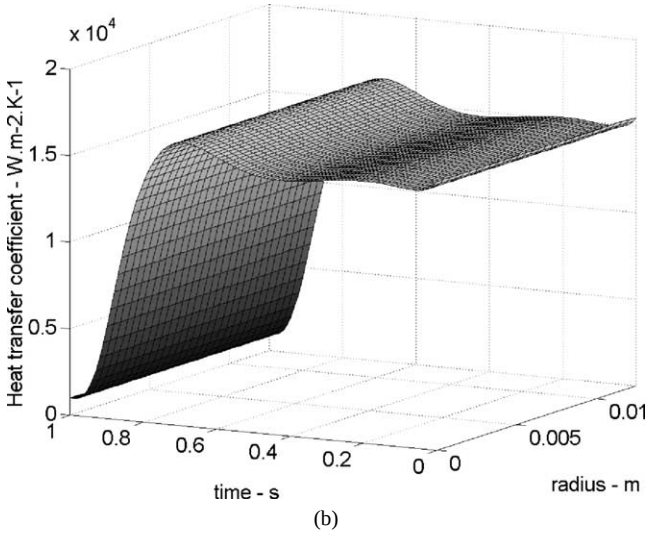

(b)

Fig. 9. (a) and (b): Values estimated in the case $H = 15\,000\ \mathrm{W{\cdot}m^{-2}{\cdot}K^{-1}}$.

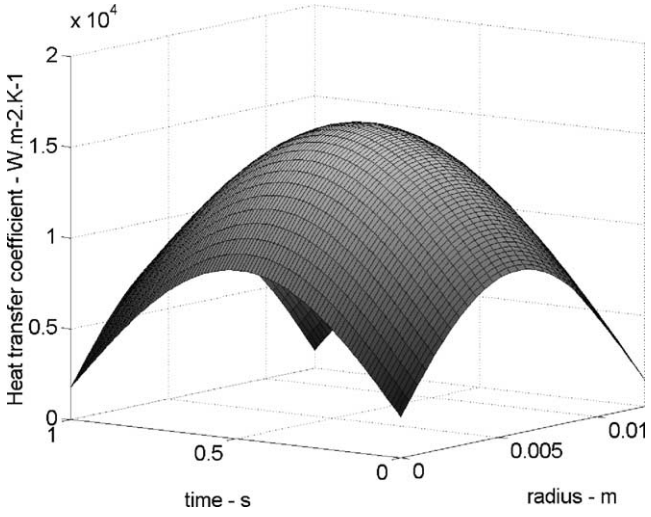

Fig. 10. Correct value to be estimated in the case of the dome.

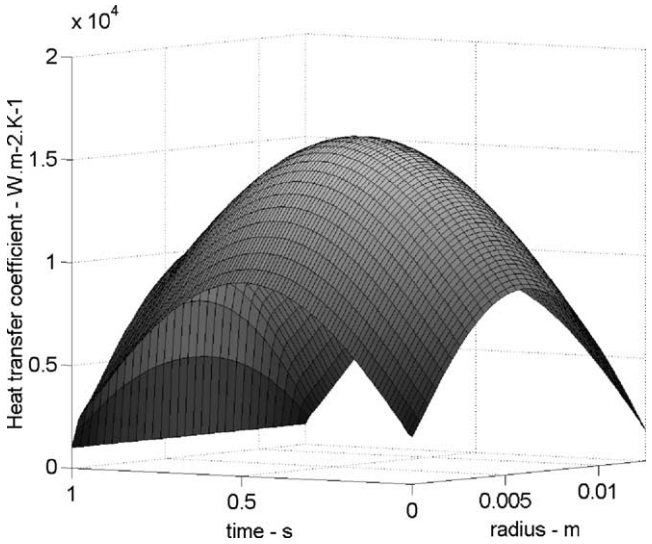

(a)

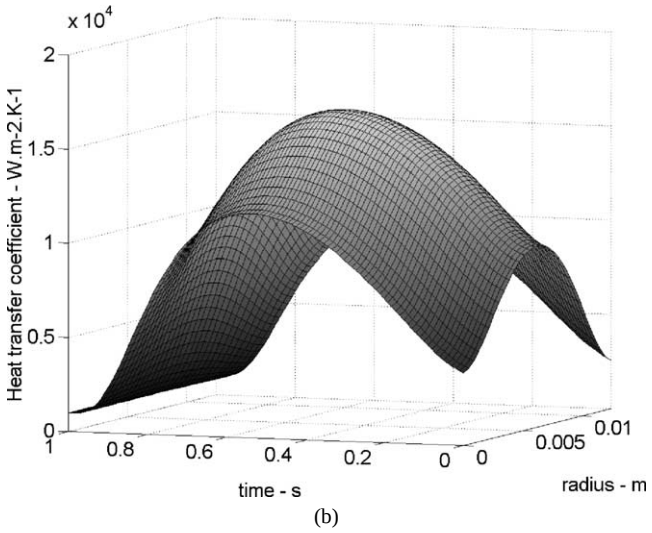

(b)

Fig. 11. (a) and (b): Values estimated in the case of the dome for $z = 0$ and $z = 1$ mm.

Figs. 13 and 14 show the results achieved in the case of the dome in $z = 0$ mm (pseudo inverse problem) and for $t_f = 1$ s. When the criterion $J(H)$ is approximately equal to δ^2 (iteration 8) the best result is obtened. Fig. 14 shows that when computing beyond the twelfth iteration, the criterion decreases, while the solution oscillates. We can see in this figure that the residues at the thirteenth iteration are bigger than the residues at the eighth iteration.

As a conclusion to this section, we can say that the estimation method, for the case of a material without any phase change and for a Fourier number equal to 0.08, gives good enough results.

5.2. *Case of 16MND5 steel*

The following test cases are analysed here:

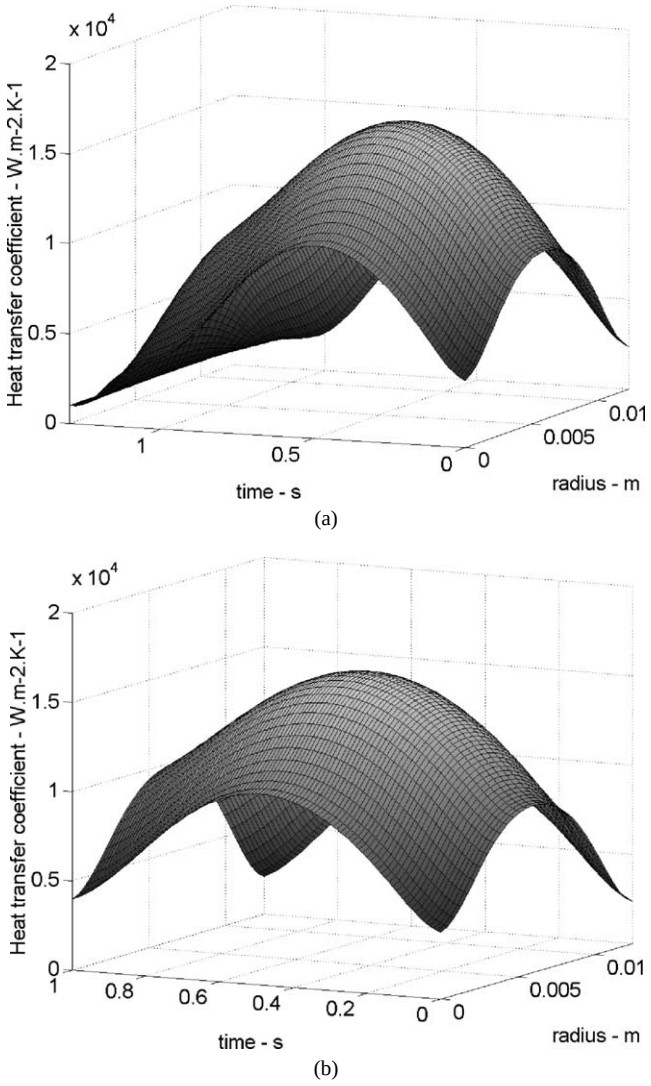

Fig. 12. (a) and (b): Values estimated in the case of the dome for $z = 1$ mm: (a) $t'_f = t_f + 30\%$; (b) truncated at t_f.

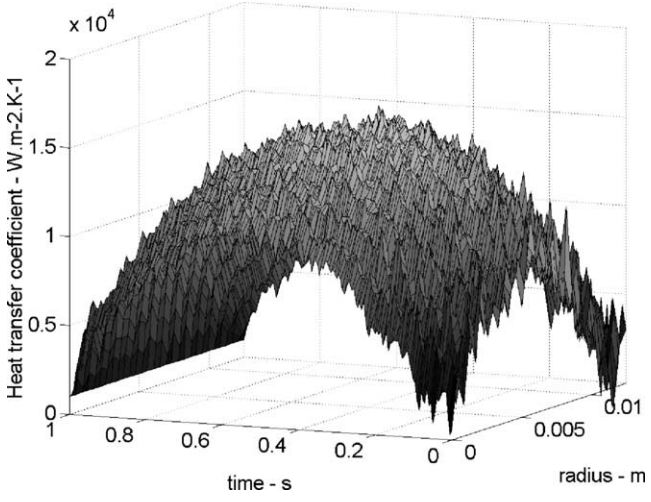

Fig. 13. Values estimated in the case of the dome for noise-added data and when $J(H) < \delta^2$ at the 8th iteration.

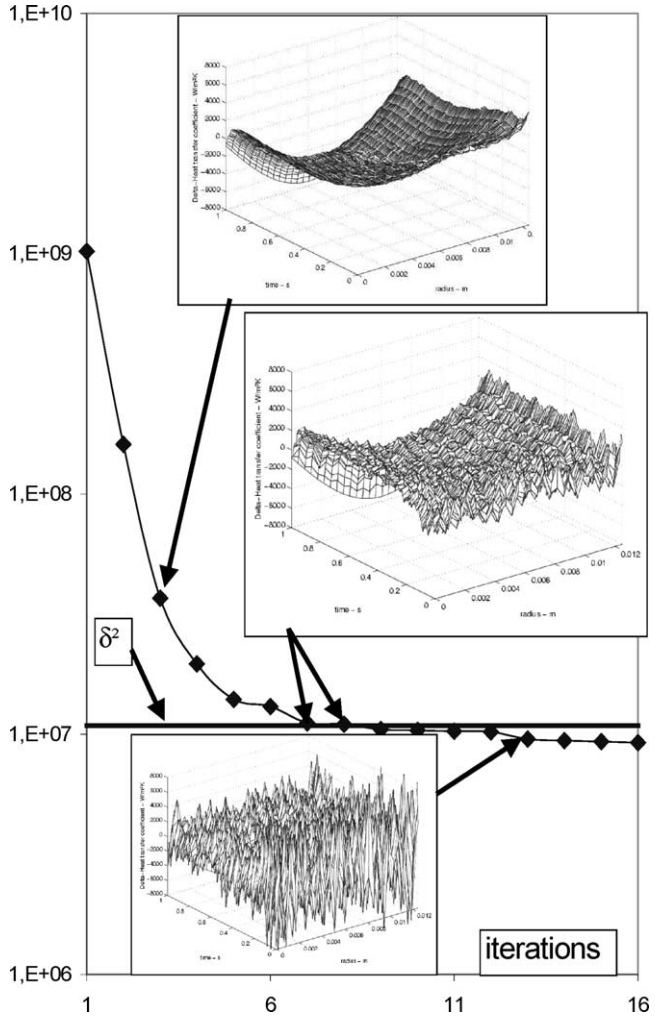

Fig. 14. Evolution of the criterion $J(H)$ and the residues.

(a) $H(r,t) = 15\,000$ W·m^{-2}·K^{-1} for $0 < r < r_{\max}$ and $0 < t < 2$ s.

(b) $H(r,t) = 5\,000 + 7\,500 \cdot (\sin(\pi t/t_{\max}) + \sin(\pi r/r_{\max}))$ for $0 < r < r_{\max}$ and $0 < t < 2$ s.

(c) $H(r,t) = H_{\exp} = H(r) \cdot H(t)$: $H_{\exp}$ (Fig. 6) designates a law of evolution of the transfer coefficient simulating the experimental reality of the Jominy test, i.e.:
- $H(t)$: A law of evolution depending on the time, which follows Sorin's curve (Fig. 3);
- $H(r)$: Weighting as a function of the radius represented by the curve in Fig. 4.

Figs. 15 and 16 display the estimates of the transfer coefficient for the case "a" from the theoretical thermal curves considered in $z = 0$ mm and $z = 1$ mm.

The results analysis shows that the iterative regularization method is not disturbed by the phase changes and that the oscillations, observed on the estimation using the function specification method [7] and the spatial regularization method [8], have disappeared. We note that $\Delta Fo = 0.04$.

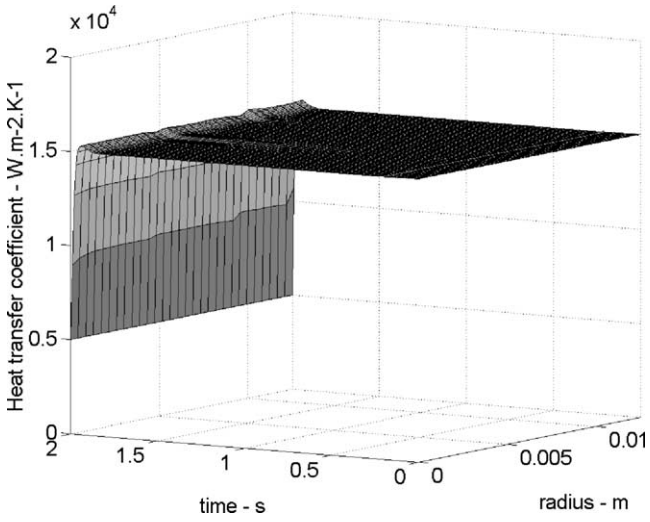

Fig. 15. Values estimated in $z = 0$ mm.

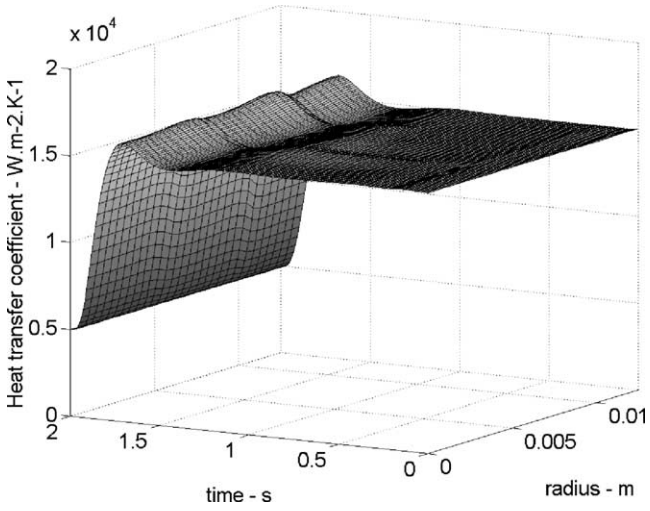

Fig. 16. Values estimated in $z = 1$ mm.

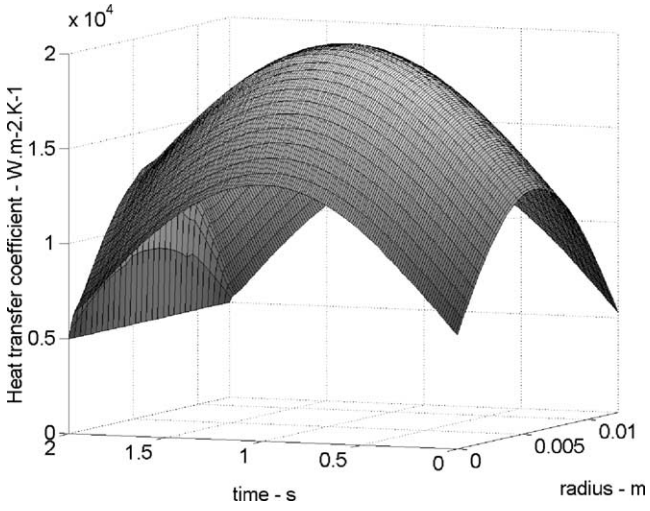

Fig. 17. Values estimated in the case of the dome from thermal cycles considered in $z = 0$ mm.

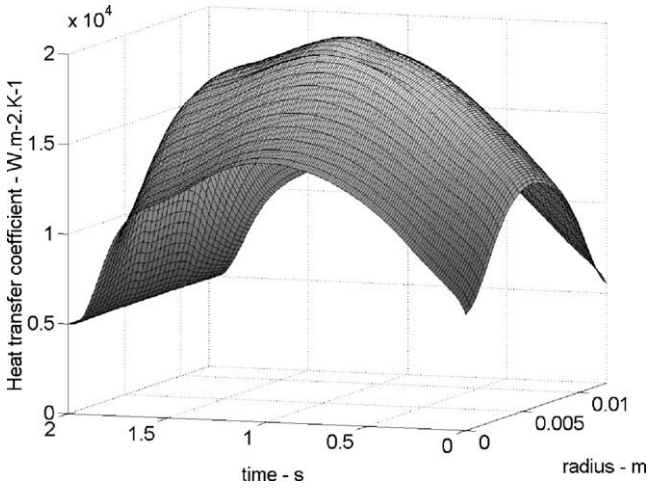

Fig. 18. Values estimated in the case of the dome from thermal cycles considered in $z = 1$ mm.

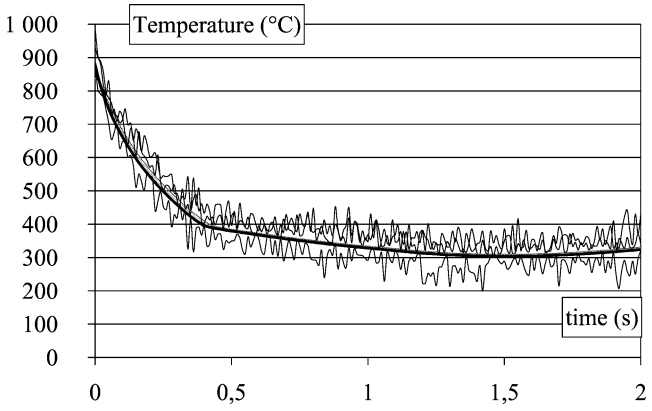

Fig. 19. Noise-added thermal cycles.

We notice the same in case “b”. Results are displayed in Figs. 17 and 18. Fig. 20 presents the results of the estimation in the case of noise-added thermal cycles (example: Fig. 19) considered in $z = 1$ mm (disturbance: $B = \omega T_{\max} \Delta_{\max}$ with $T_{\max} = 880\,^{\circ}\mathrm{C}$ and $\Delta_{\max} = 5\%$).

Fifteen iterations are necessary to reach the value δ^2 of the residual functional (8).

The last case tested is case “c” represented in Fig. 6. The different phases connected to vaporization, boiling and forced convection can also be found here. If we take the thermal cycles at $z = 0$ mm, we show that the estimation results are correct apart from $t = t_f$ on $z = 0$ mm (Fig. 21).

Fig. 22 is plotted from the thermal cycles considered in $z = 1$ mm. We note that the damping effect due to depth generates the lowering of the boiling peak of $H_{\exp}$.

When noise is added to the thermal cycles as previously, the estimated values (Fig. 23 for $z = 0$ mm and Fig. 24 for $z = 1$ mm) remain satisfactory. Plating, however, is observed on the function $H_{\exp}$. When the criterion $J(H)$ is equal δ^2, the estimation stop.

The last result (Fig. 25) we present here is a test where no noise has been added relating to estimations for thermal

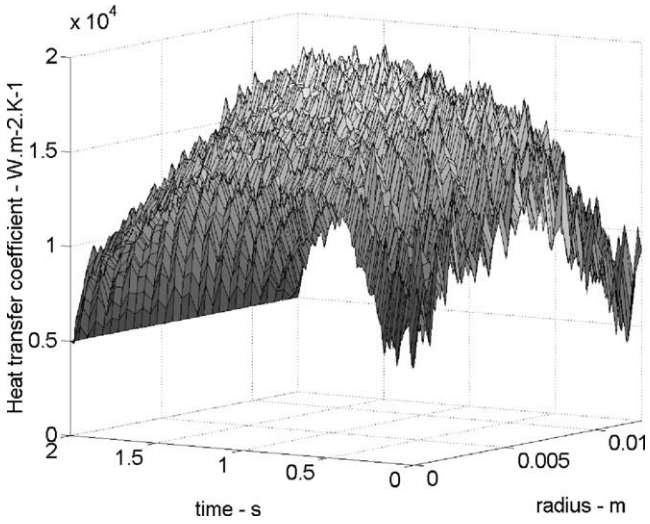

Fig. 20. Values estimated from noise-added thermal cycles considered in $z = 1$ mm.

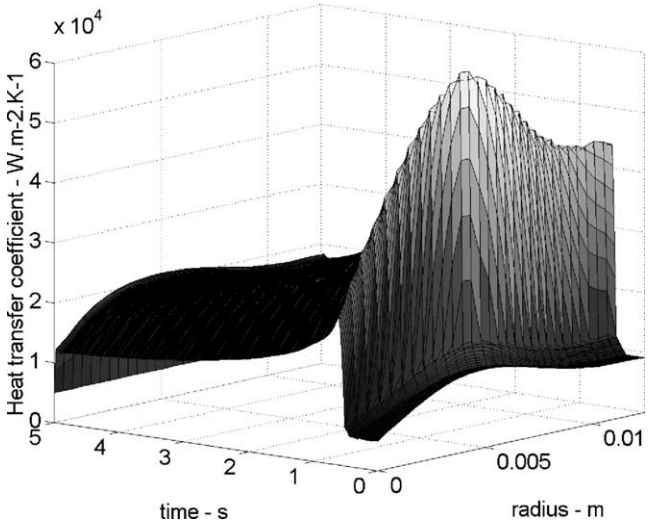

Fig. 21. Values estimated from the thermal cycles considered in $z = 1$ mm.

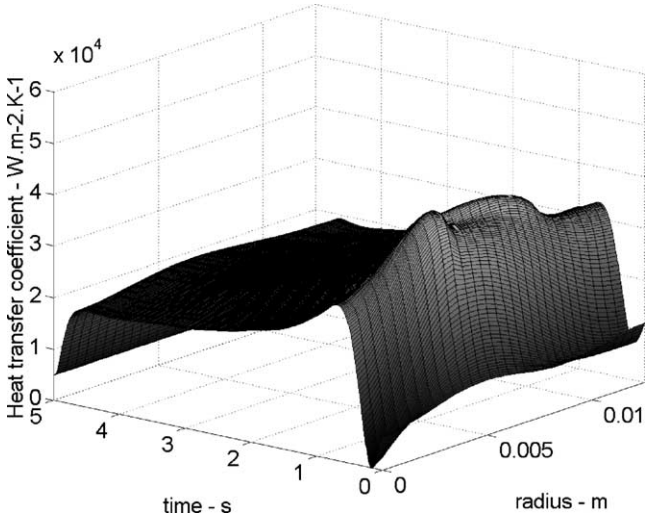

Fig. 22. Values estimated from the thermal cycles considered in $z = 0$ mm.

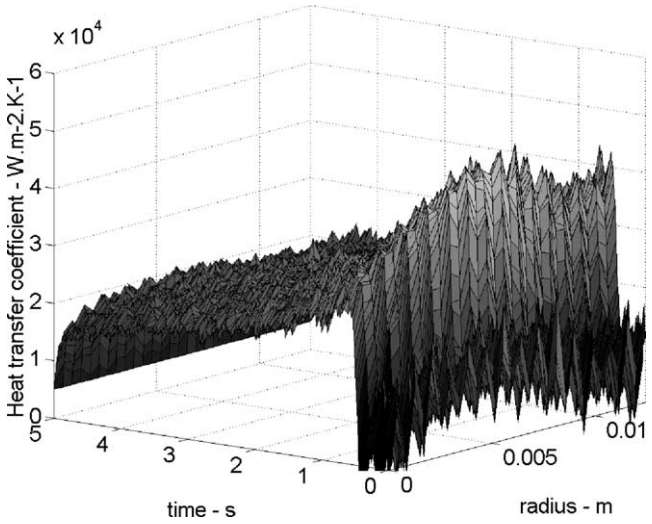

Fig. 23. Values estimated from the noise-added thermal cycles considered in $z = 1$ mm.

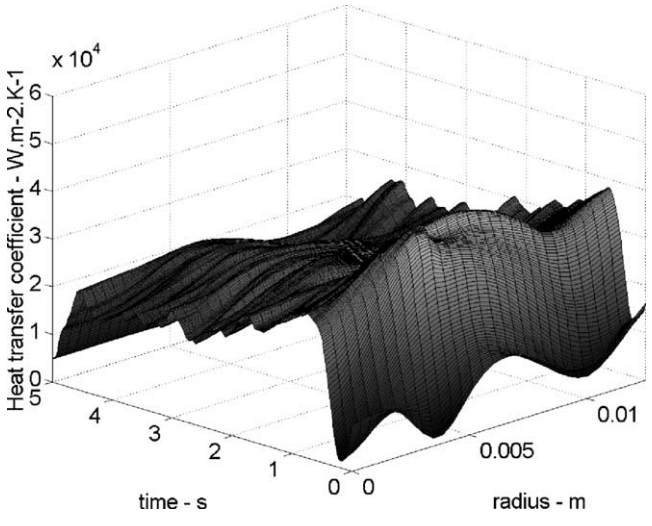

Fig. 24. Values estimated from the thermal cycles considered in $z = 0.6$ mm and $N = 8$.

cycles considered in $z = 0.6$ mm at few measurement points in the radial direction $N = 8$ (eight thermocouples distributed according to thirty space grid nodes.

The 8 experimental thermal cycles can be used afterwards with a spline cubic base to define the thermal cycles at all space grid nodes.

6. Conclusion

The objective of this research was the estimation of a high two-d transient heat transfer coefficient during the quench-end metallurgical test by solving a nonlinear inverse heat conduction problem. By using the function specification method, this problem has been found to be difficult to solve and the obtained results show a big instabilities [3,6]. The inherent huge nonlinearities of thermophysical properties of

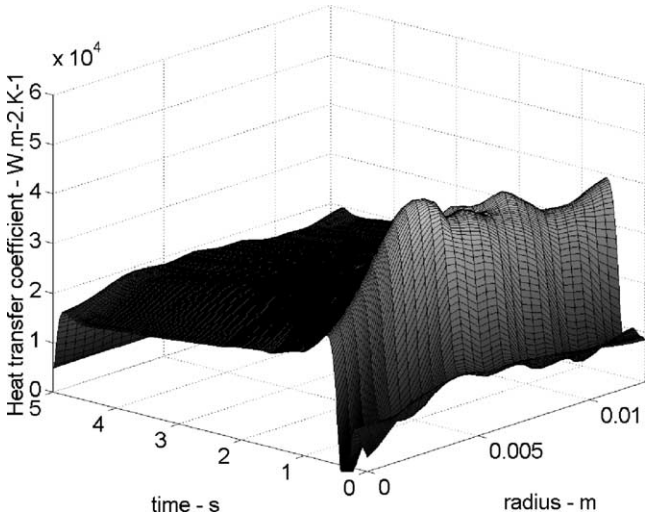

Fig. 25. Values estimated from the thermal cycles considered in $z = 0.6$ mm and $N = 8$.

the material under investigation are at the origin of these instabilities.

In the presented study, the conjugate gradient method coupled to the adjoint state equations approach was used in the resolution of this problem. The stabilization of the results was obtained by the iterative regularization method. The developed algorithm with the discreapancy principle seem to give a better results that the function specification method even with a relatively weak Delta Fourier number.

References

[1] Manuel d'utilisation "SYSWELD", Systus International, 1994.
[2] P. Le Masson, P. Rogeon, D. Carron, J.J. Quemener, Simulation numérique thermométallurgique : Influence des paramètres d'entrée sur la modélisation d'un essai de trempabilité, in: Revue de Métallurgie – CIT/Sciences et Génie des Matériaux, 2000, pp. 1055–1064.
[3] P. Le Masson, P. Rogeon, D. Carron, J.J. Quemener, Identification du coefficient de transfert lors d'un essai Jominy instrumenté, SFT 99 (1999) 57–62.
[4] A. Osman, J.V. Beck, Investigation of transient heat transfer coefficient in quenching experiments, J. Heat Transfer 112 (1990) 843–848.
[5] S.G. Chen, C.I. Weng, J. Lin, Inverse estimation of transient temperature distribution in the end quenching test, J. Mater. Proces. Technol. 86 (1999) 257–263.
[6] P. Archambault, S. Denis, A. Azim, Inverse resolution of the heat transfer equation with internal heat source: Application to the quenching of steels with phase transformations, J. Mat. Engrg. Perf. 6 (1997) 240–246.
[7] J.V. Beck, B. Blackwell, C.R. St. Clair, Inverse Heat Conduction Ill-Posed Problem, Wiley, New York, 1985.
[8] A.N. Tikhonov, V.Y. Arsenin, Solutions of Ill-Posed Problems, Winston, Washington, DC, 1977.
[9] G. Blanc, M. Raynaud, The Hiep Chau; A guide for the use of the function specification method for 2D Inverse heat conduction problems, Rev. Gén. Therm. 37 (1998) 17–30.
[10] G. Blanc, Problème inverse multidimensionnel de conduction de la chaleur: Optimisation du positionnement des capteurs et utilisation des mesures de thermo-déformations, Thèse de doctorat, INSA de Lyon, 18 Janvier, 1996.
[11] O.M. Alifanov, E.A. Artyukhin, S.V. Rumyantsev, Extreme Methods for Solving Ill-Posed Problems with Applications to Inverse Heat Transfer Problems, Begell House, New-York, 1995.
[12] O.M. Alifanov, N.V. Kerov, Determination of external load parameters by solving the two-dimensional inverse heat-conduction problem, Inzhenerno-Fizicheskii Zhurnal 41 (4) (1981) 581–586, translated.
[13] O.M. Alifanov, A.V. Nenarokomov, Boundary inverse heat conduction problem in extreme formulation, in: Inverse Problems in Engineering: Theory and Practice, ASME, 1993.
[14] R. Abou Khachfe, Y. Jarny, Numerical solution of 2-D non linear inverse heat conduction problems using finite element techniques, Numer. Heat Transfer B 37 (2000) 45–68.
[15] Essai de trempabilité Jominy, NFA 04-303, Juin, 1979.
[16] Atlas de courbes Jominy (états bruts de trempe et revenus) d'aciers de la norme NFA 35-552; Collection ATS OTUA—Propriétés d'emploi des aciers: renseignements techniques; Paris, 1985.
[17] J.B. Leblond, J. Devaux, A new kinetic model for anisothermal metallurgical transformations in steels including effect of austenite grain size, Acta Metall. 32 (1) (1984) 137–146.
[18] D.P. Koistinen, R.E. Marburger, A general equation describing, Acta. Metall. 7 (1959) 59.
[19] A. Sorin, Modélisation des conditions de refroidissement d'une éprouvette Jominy; Rapport de stage—Centre d'Etude des Structures et des Matériaux Navals (CESMAN), Juin 1997.
[20] D. Hömberg, A numerical simulation of the Jominy end-quench test, Acta Mater. 44 (1996) 4375–4385.
[21] M.N. Ozisik, Heat Conduction, Wiley Sons, New York, 1993.
[22] E. Polak, Computational Methods in Optimization, Academic Press, New York, 1993.